A NEW TORQUE AND FLUX CONTROLLERS FOR DIRECT TORQUE CONTROL OF INDUCTION MACHINES

N. R.N Idris* & T.C. Ling
Electrical Energy Conversion Dept
Universiti Teknologi Malaysia
81310 UTM, Skudai, Malaysia
*Email: nikrumzi@ieee.org

Malik E. Elbuluk
Dept. of Electrical & Comp. Engineering
University of Akron
Akron, OH 44325-3904, USA
Email: melbuluk@uakron.edu

Abstract:--This paper presents the implementation of a high performance Direct Torque Control (DTC) of induction machines drive. DTC has two major problems, namely. high torque ripple and variable switching frequency. In order to solve these problems, this paper proposed a pair of torque and flux controllers to replace the hysteresis-based controllers. The design of these controllers is fully discussed and a set of numerical values of the parameters for the proposed controllers is given. The simulation of the proposed controllers applied to the DTC drive is presented. The simulation results are then verified by experimental results. The hardware implementation is mainly constructed by using DSP TMS320C31 and Altera FPGA devices. The results prove that a significant torque and stator flux ripples reduction is achieved. Likewise, the switching frequency is fixed at 10.4 kHz and a more sinusoidal phase current is obtained.

I. INTRODUCTION

Not until mid 1980's, when Direct Torque Control (DTC) was first introduced, field-oriented control (FOC) of induction machines was considered the only scheme capable of delivering high performance torque control in AC machines [1]. The first DTC drive was marketed by ABB in 1996, and since then has gained popularity in applications which previously have utilized FOC drives. In DTC, the torque and flux are directly controlled using optimum voltage vectors, whereas the FOC which uses *q*- and *d-axis* components of the stator current to control the torque and flux respectively, and require current regulated Pulse Width Modulation (PWM) or Space Vector Modulation (SVM) for implementation. Unlike the FOC drives, where frame transformation is a must, no frame transformation is required in DTC, and in its basic configuration, only the stator resistance is required to estimate the stator flux and torque. It is also shown that DTC of induction machine gives faster torque response compared to the FOC of induction machines. The basic configuration of the conventional DTC drive consists of a pair of hysteresis comparator, torque and flux estimators, voltage vector selector and a Voltage Source Inverter (VSI). Although gaining popularity, DTC has some drawbacks, which need to be rectified. Variable switching frequency and high torque and flux ripples are the major problems.

The root of variable switching frequency in DTC is the use of torque and flux hysteresis controllers, as originally proposed in [1]. Hysteresis controllers not only produce variable switching frequency but also produce in large torque and flux ripples. Therefore, various methods have been proposed to overcome these problems including the use of variable hysteresis bands [2], predictive control schemes [3], space vector modulation [4] and intelligent control techniques [5]. The use of these techniques however, have somehow increased the complexity of the control technique in DTC and diminished the main feature of DTC, which is simple control structure.

A torque controller, which produces constant torque switching frequency with low ripple, has been presented in [6]. It replaces the convention hysteresis comparator with a fixed switching frequency controller. A fixed switching frequency is obtained by comparing the triangular waveforms with the compensated error signals. However, there are two major limitations associated with this method. Firstly, the switching frequency is limited by the sampling period of the processor. Secondly, the switching frequency still varies due to the flux hysteresis comparator.

This paper expands on the work presented in [6]. It presents a torque and flux controllers to replace the hysteresis-based controllers. the hardware implementation of our proposed controllers. The design of the controllers is fully discussed and a set of numerical values of the parameters for the proposed controllers is given. The simulation of the proposed controllers applied to the DTC drive is presented and compared with the hysteresis-based controller. The simulation results are verified by experimental results. The hardware implementation is mainly constructed by using DSP TMS320C31 and Altera FPGA devices. Due to the principle of the controllers, which is based on waveform comparisons, the implementation is relatively easy. The FPGA device was used to perform the waveform comparisons and the DSP was used to estimate the torque and stator flux. Section III presents the principle and modeling of the proposed controllers. Section IV discusses on the design and implementation of the controllers with the simulation and experimental results.

II. PROPOSED TORQUE AND FLUX CONTROLLERS

The proposed DTC consists of two controllers; namely a torque controller and a flux controller, as shown in

Figure 1. The operations of the new torque and flux controllers are similar to the torque controller proposed in [6] but with a much higher triangular carriers frequency. The maximum switching capability of the devices can be fully utilized since the switching frequency is independent of the operating conditions and equals the triangular waveform frequency. These controllers are easy to implement by utilizing digital circuit since it just involves comparison of waveform rather than complicated calculation of duty cycles or voltage vector.

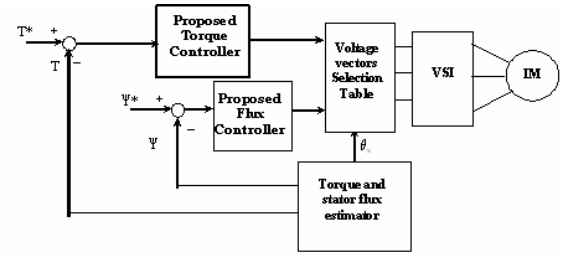

Fig. 1 DTC drive with the proposed torque and flux controllers

A. Torque controller

The proposed torque controller consists of two triangular waveform generators, two comparators and a PI controller as shown in Figure 2. The two triangular waveforms (C_{upper} and C_{lower}) are 180° out of phase with each other. The absolute values of the DC offsets for the triangular waveforms are set to half of their peak-peak values.

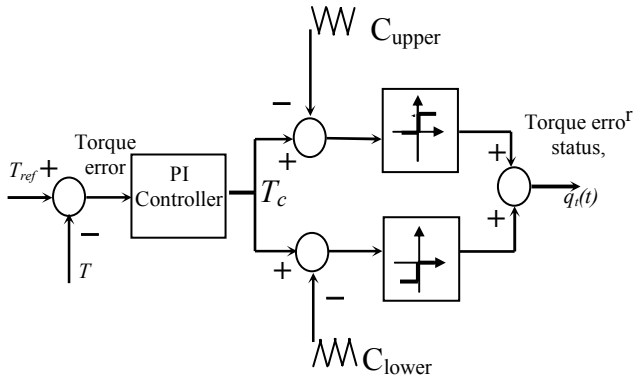

Figure 2 Proposed Torque Controller

The instantaneous output of the proposed torque controller, $q_t(t)$ is same as the three level hysteresis comparator [3] that can be one of the three states: –1, 0 or 1 with the following conditions.

$$q_t(t) = \begin{cases} 1 & for\ T_c \geq C_{upper} \\ 0 & for\ C_{lower} < T_c < C_{upper} \\ -1 & for\ T_c \leq C_{lower} \end{cases} \quad (1)$$

The average torque error status is defined as continuous duty ratio and is denoted by $d_t(t)$. taken over an interval T_{tri}, which is the period of the triangular carrier waveform.

$$d_t(t) = \frac{1}{T_{tri}} \int_{t}^{t+T_{tri}} q_t(t)\, dt \quad (2)$$

In order to properly design the PI controller, a small signal model of the torque loop has to be developed. The space vector equations of induction machine expressed in general rotating frame are given by:

$$\bar{v}_s^g = R_s \bar{i}_s^g + \frac{d\bar{\psi}_s^g}{dt} + j\omega_g \bar{\psi}_s^g \quad (3)$$

$$0 = R_r \bar{i}_r^g + \frac{d\bar{\psi}_r^g}{dt} + j(\omega_g - \omega_r)\bar{\psi}_r^g \quad (4)$$

In the equations (3) and (4) , $\bar{\psi}_s^g$ and $\bar{\psi}_r^g$ are the stator and rotor flux linkages respectively and are given by:

$$\bar{\psi}_s^g = L_s \bar{i}_s^g + L_m \bar{i}_r^g \quad (5)$$

$$\bar{\psi}_r^g = L_r \bar{i}_r^g + L_m \bar{i}_s^g \quad (6)$$

The super-script ‘g’ in the above equations denotes that the quantity is referred to the general reference frame. The torque and mechanical dynamics of the machines are modeled by the following:

$$T_e = \frac{3}{2}\frac{p}{2} \bar{\psi}_s^g \times \bar{i}_s^g \quad (7)$$

$$J\frac{d\omega_m}{dt} = J\frac{2}{p}\frac{d\omega_r}{dt} = T_e - T_{load} \quad (8)$$

It has been shown in our previous paper [6] that using the space vector equations of the induction machine given in (3)-(6), the positive and negative torque slopes in stator flux reference frame can be written as:

$$\frac{dT_e^+}{dt} = -\frac{T_e}{\sigma\tau_{sr}} + \frac{3p}{4}\frac{L_m}{\sigma L_s L_r}\left[v_s^{\psi s}\psi_s - (\omega_r - \omega_{\psi_s})\cdot(\psi_s \psi_r^{\psi s})\right] \quad (9)$$

$$\frac{dT_e^-}{dt} = -\frac{T_e}{\sigma\tau_{sr}} - \frac{3p}{4}\frac{L_m}{\sigma L_s L_r}\left[(\omega_r - \omega_{\psi S})\cdot(\psi_s \psi_r^{\psi S})\right] \quad (10)$$

The superscript $\omega_{\psi s}$ in (9) and (10) indicates that quantities are referred to the stator flux reference frame and $\frac{1}{\sigma\tau_{sr}} = \left(\frac{1}{\sigma\tau_s} + \frac{1}{\sigma\tau_r}\right)$, where σ, τ_s , τ_r are the total leakage factor, stator time constant and rotor time constant respectively. Since we know that the number of active voltage vectors selected over one synchronous cycle is given by $2\pi f_{tri}/\omega_e$, where ω_e is the synchronous frequency and f_{tri} is the triangular frequency, the ratio between the small change in stator flux angle ($\Delta\theta$) and the duration of active voltage vectors applied (Δt) is given by:

$$\frac{\Delta\theta}{\Delta t} = \frac{\left(\frac{2\pi\omega_e}{2\pi f_{tri}}\right)}{\frac{d_t}{f_{tri}}} = \frac{\omega_e}{d_t} \quad (11)$$

Assuming that Δt is small enough such that the change in stator flux is linear, (11) approximates $\omega_{\psi s}$; i.e. $\omega_{\psi s}\, d = \omega_e$ Therefore the instantaneous stator flux frequency can be

written in terms of average duty ratio d_t and rotor speed as:

$$\omega_{\psi s} = \frac{\omega_{slip} + \omega_r}{d_t} \tag{12}$$

Substituting (12) into (9) and (10) and averaging these equations [6] gives:

$$\frac{dT_e}{dt} = -A_t T_e + B_t v_s^{\psi s} d + K_t(\omega_{slip}) \tag{13}$$

where $A_t = \frac{1}{\sigma\tau_{sr}}$, $B_t = \frac{3p}{4}\frac{L_m}{\sigma L_s L_r}\psi_s$, $K_t = \frac{3p}{4}\frac{L_m}{\sigma L_s L_r}(\psi_s \psi_r^{\psi_s})$

In (13) it is assumed that the magnitudes of the stator and rotor fluxes are held constant. Equation (13) can now be transformed to frequency domain and linearized by introducing small perturbation in T_e, d_t and ω_{slip}. The torque, T_e therefore can be written as:

$$\tilde{T}_e(s) = \frac{B_t v_s^{\psi s}\tilde{d}_t(s) + K_t\tilde{\omega}_{slip}(s)}{s + A_t} \tag{14}$$

The term contributed by the slip frequency is relatively small and hence for simplicity will be neglected. The small signal torque loop is shown in Fig 3. Ideally, the torque loop bandwidth should be as large as possible to obtain fast torque response. However, the bandwidth and hence the selection of controller's parameters (proportional gain K_{tp}, and integral gain K_{ti}) is limited by either the triangular frequency or the sampling period, depending on which one is lower. This means that we can increase the inverter switching frequency much higher than the sampling frequency provided that the bandwidth is limited by the sampling frequency. Since the triangular waveform is generated using the FPGA device, its frequency can be few times higher than the sampling frequency. It is, however, necessary to synchronize the sampling and the triangular waveforms.

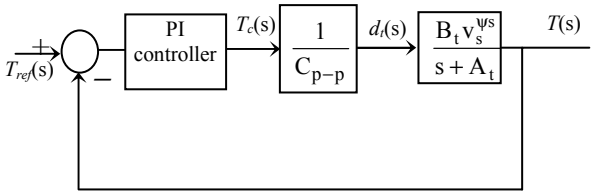

Fig. 3 Small signal torque loop

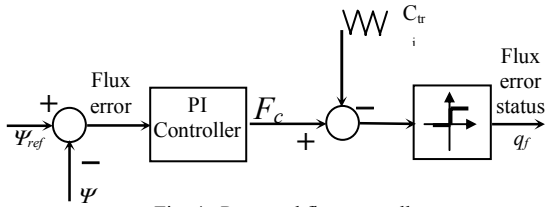

Fig. 4 Proposed flux controller

B. Flux Controller

The proposed flux controller is shown in Fig 4, which in principle works similar to that of the torque controller. As in the hysteresis-based controller, there are only two levels of output generated from the controller, i.e. 1 to increase the flux and 0 to reduce the flux. This implies that only single triangular waveform is required. For a given synchronous frequency, the switching frequency of the flux controller only depends on the triangular waveform frequency. The output of the controller is given by:

$$q_f(t) = \begin{cases} 1 & \text{for } F_c \geq C_{tri} \\ 0 & \text{for } F_c < C_{tri} \end{cases} \tag{15}$$

For a triangular period of T_{tri}, its average value is given by:

$$d_f(t) = \frac{1}{T_{tri,f}} \int_t^{t+T_{tri,f}} q(t)\, dt \tag{16}$$

For the sake of simplicity, we will assume that the stator resistance drop is negligible, hence using (3), the slope of the flux in stationary reference frame can be approximated by (17) which simply indicate that it is totally depends on the selected voltage vectors.

$$\text{slope} \equiv \frac{d\overline{\Psi}}{dt} = \overline{v}_s \tag{17}$$

The derivative of the stator flux vector at *t* is the tangent vector of the stator flux to the curve traced by $\overline{\psi}_s$ at *t*. Therefore the slope depends on the stator flux position and it can be seen from Fig. 5 that at every entrance of a sector, the magnitude of the positive and negative slopes are zero and maximum, respectively.

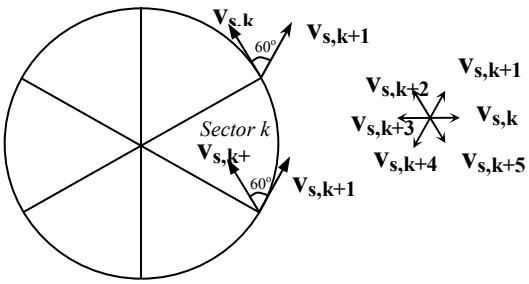

Fig.5 Circular flux locus

If θ is the angle of the stator flux relative to the sector it enters, the positive and negative slopes can be written as:

$$\left.\begin{aligned} \text{slope}^+ &\equiv \frac{2}{3} V_{dc} \sin\theta \\ \text{slope}^- &\equiv -\frac{2}{3} V_{dc} \sin(\theta + \frac{2}{3}\pi) \end{aligned}\right\} \tag{18}$$

For simplicity it will be assumed that the slope is constant during which the flux error status is 1 or 0. Then, it is possible to obtain the average positive and negative slopes by averaging them over a sector. This is easily done since we know the number of positive or negative slopes within a sector is given by $N_f = (2\pi f_{tri})/6\omega_e$. The average positive and negative slope can be calculated as:

$$\frac{d\Psi^+}{dt} = \frac{1}{N_f}\sum_{n=0}^{N_f}\frac{2}{3}V_{dc}\sin\left(\frac{\frac{\pi}{3}}{N_f}\right)n = A_\psi \tag{19}$$

$$\frac{d\Psi^-}{dt} = -\frac{1}{N_f}\sum_{n=0}^{N_f}\frac{2}{3}V_{dc}\sin\left(\left(\frac{\frac{\pi}{3}}{N_f}\right)n + \frac{2}{3}\pi\right) = B_\psi \tag{20}$$

Which gives an average slope of:

$$\frac{d\Psi}{dt} = (A_\psi - B_\psi)d_f + B_\psi \quad (21)$$

Introducing small perturbation in ψ and d_f, the transfer function between ψ and d can be obtained as:

$$\frac{\tilde{\Psi}}{\tilde{d}_f} = \frac{(A_\psi - B_\psi)}{s} \quad (22)$$

Finally, the small signal flux loop is shown as in Fig 6.

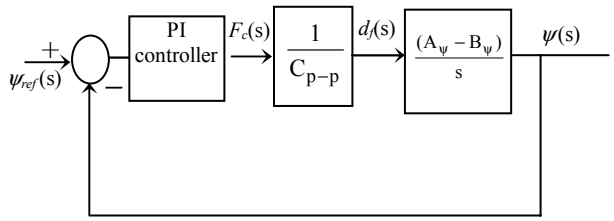

Fig. 6 Small signal flux loop

It is clear from the small signal model that only proportional type controller is required to obtain zero steady state error in flux response. Similar to torque control, the bandwidth is limited by the triangular frequency or the sampling frequency, depending on which one is lower. Provided that the sampling is synchronized with the triangular waveform, the switching frequency can be made higher than the bandwidth of the flux loop.

III. SIMULATION, IMPLEMENTATION RESULTS AND DISCUSSIONS

Three different sets of simulations and experiments were carried out as follows:

i) Hysteresis torque and flux controllers,
ii) Proposed torque controller and hysteresis flux
iii) Proposed torque and flux controllers

The simulations of the DTC drive were carried out using Matlab/Simulink simulation package. The parameters of the induction machine used in the simulation and experiment are listed in Table I.

TABLE I
PARAMETERS OF INDUCTION MACHINE AND SETTINGS

Stator resistance	10.9 Ω
Rotor resistance	9.5 Ω
Stator self inductance	0.859 H
Rotor self inductance	0.859 H
Mutual inductance	0.828 H
Rated speed	2880 rpm
Pole pair	2
DC link voltage	120 V
Rated flux	0.495 Wb

Using the design procedure described in Section II, proportional and integral constants for the PI torque controller were calculated as $K_p = 180$ and $K_i = 6000$. With these values, the torque loop bandwidth is found out to be 1885 rad/s. For this particular design, the bandwidth is limited by the triangular frequency, since the triangular frequency is lower than the sampling frequency. It should be noted that it is possible to increase the inverter switching frequency higher than the DSP sampling frequency by increasing the triangular frequency. Under this condition, the controller should be designed such that the bandwidth is constrained by the DSP sampling frequency. As for the flux loop bandwidth, it can be adjusted by simply varying the gain of the flux proportional controller. It was found out that the value of K_{pf}=11000 gives flux bandwidth of 15268 rad/s.

A. Implementation of the Proposed Controllers

The major parts of the controllers were composed of a DSP and an FPGA device. With this combination, it is possible to generate the triangular waveforms at frequencies close to or higher than the sampling frequency of the DSP. Therefore as discussed in the previous section, it is possible to increase the switching frequency of the inverter much higher than the sampling period.

The DSP board (DS1102) from dSPACE, based on TMS320C31 operating at 60 MHz, was used in this paper. It was mainly used to estimate the torque and stator flux using the stator current and voltage, which were sampled at 20.8 kHz (DSP sampling period T_{DSP} = 48μs) . Other than this, the DSP was also responsible for 1) implementing the PI and P controllers for the torque and flux loops, respectively and 2) determining the sector of the stator flux. These values were then passed to the Altera EPF10K20 FPGA device contained on an Altera UP1 Educational Board. Very high-speed integrated circuits Hardware Description Language (VHDL) was utilized in digital logic designs of the FPGA. The design was then compiled and simulated using MAX + PLUS II and finally downloaded to the EPF10K20 device. Since the triangular waveforms of the torque and flux controllers were generated using FPGA, their frequencies were not constrained by the clock speed of the DSP. In this paper, the torque and flux triangular frequencies are set to 10.4 kHz and 5.2 kHz, respectively and they are synchronized with the sampling frequency of the DSP – this is illustrated in Fig. 7.

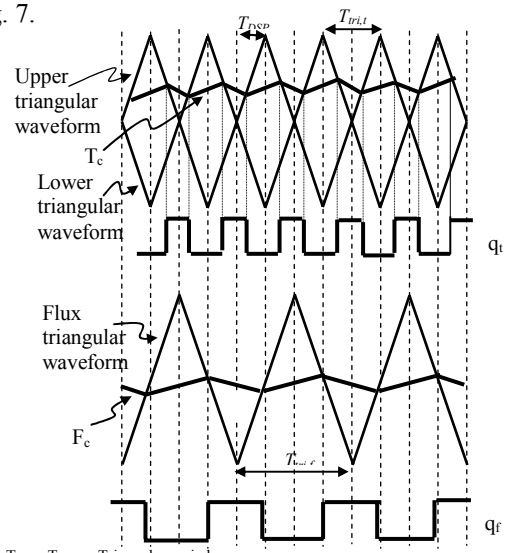

Fig. 7 Ideal timing diagram of the proposed torque and flux controllers

The torque and flux errors which were obtained from the DSP, were compared with the triangular waveforms within the FPGA. From the comparison results and the location of the stator flux, suitable voltage vectors were selected. The various tasks of the DSP and the FPGA were summarized in Fig. 8.

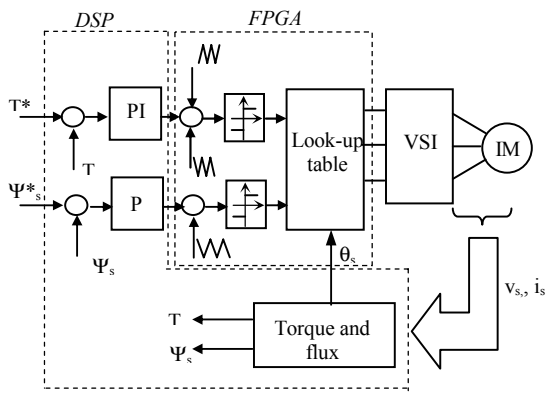

Fig. 8 Implementation of the proposed controllers using DSP and FPGA

B. *Results and Discussions*

Fig. 9 shows the simulation and experimental results of a torque response for a step reference step from -0.6 Nm to 0.6 Nm. Experimental results for the torque and flux hysteresis controllers shows a significant ripple due to the sampling delay in the DSP. This cannot be seen in the simulation since the model does not include the sampling delay. All of the three sets of controllers show an excellent torque response, however the ones with the proposed torque controller produce significant torque ripple reduction. Fig. 10 shows the steady state current and line-line voltage for the three different sets of controllers. The corresponding steady state stator flux locus is shown in Fig. 11. Clearly, with the proposed torque and flux controllers, current distortion and stator flux ripple are significantly reduced.

To examine the dynamics of the proposed controllers, a speed loop was constructed using a low resolution incremental encoder as a speed sensor (200 ppr). A square wave speed reference was applied and the experimental results of the speed and torque responses are shown in Fig. 12. The figure clearly indicates an excellent dynamic performance of the proposed controller with significant torque ripple reduction.

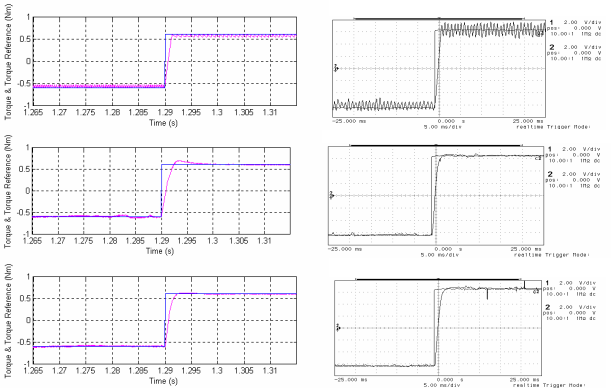

Fig. 9 Step torque response. Experimental results scale of 0,2 Nm/div. (a) hysteresis torque and flux controllers, (b) Proposed torque and hysteresis flux controllers, (c) proposed torque and flux controllers.

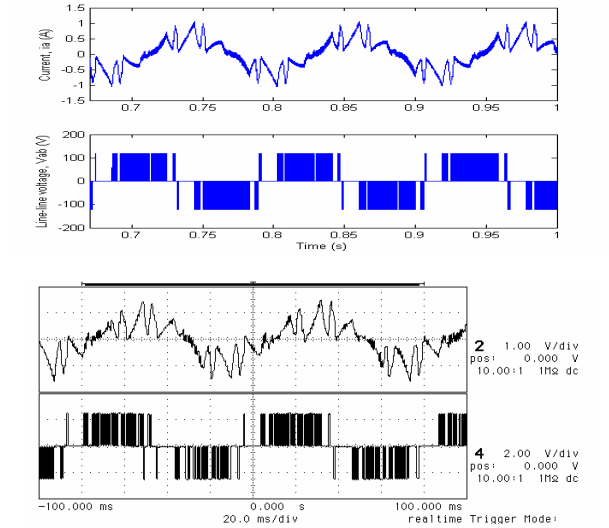

(a)

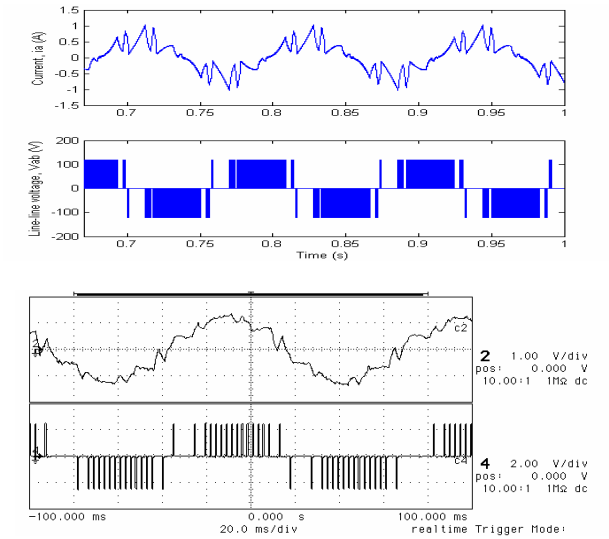

(b)

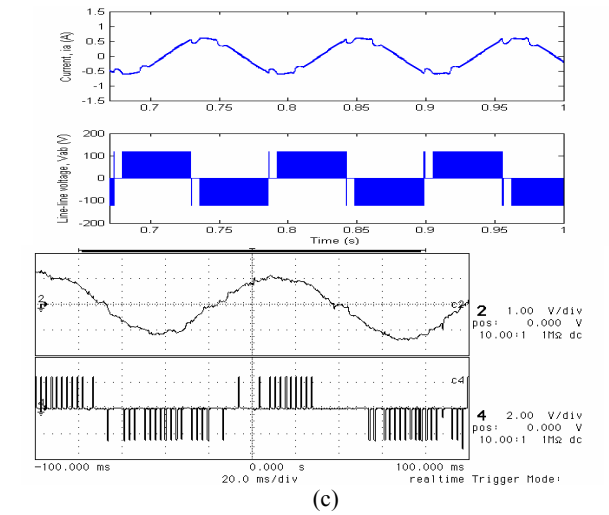

(c)

Fig.10 Simulation and experimental (0.5714A/div, 100V/div) results of steady state phase current and line-line voltage. (a) Hysteresis-based torque and flux controllers, (b) Proposed torque and hysteresis-based flux controllers, (c) Proposed torque and flux controllers

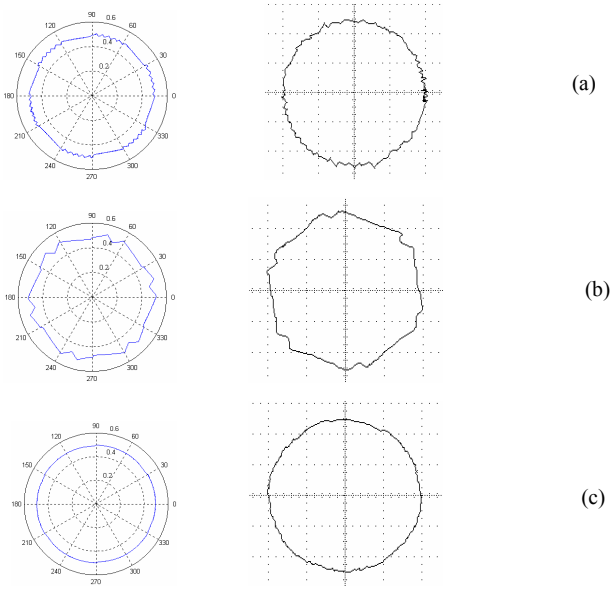

(a)

(b)

(c)

Fig. 11 Simulation and experimental stator flux locus (0.2 Wb/div) for (a) Hysteresis-based torque and flux controllers, (b) Proposed torque and hysteresis-based flux controllers, (c) Proposed torque and flux controllers

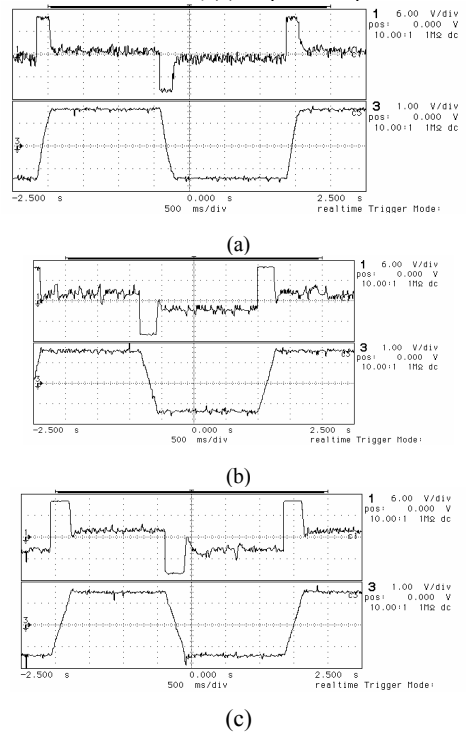

(a)

(b)

(c)

Fig. 12 Experimental results. Torque (1 Nm/div) and speed (9.33 rad/s/div) response with square wave speed reference. (a) Hysteresis torque and flux controllers, (b) Proposed torque and hysteresis-based flux controllers, (c) Proposed torque and flux controllers

Finally, to look at the switching frequency of the inverter, a square wave torque reference of ±0.6 Nm was applied and the frequency spectrum of a switching leg was recorded as in Fig. 13. The hysteresis-based controller produced an unpredictable and dispersed switching harmonics, whereas for the proposed controllers, the harmonic component is concentrated around the carrier frequency and its multiple. The first harmonic appeared at 10.4 kHz, which is equivalent to the torque loop triangular waveform frequency.

IV. CONCLUSIONS

The paper has presented the new torque and flux controllers with constant switching frequencies. Small signal modeling of the torque and flux loops has been presented. The simulation and implementation of the DTC drive with the proposed controllers were presented. From the simulation and experimental results, it is shown that despite of their simple control structure and implementation, the proposed controllers have managed to significantly reduce the torque and flux ripples.

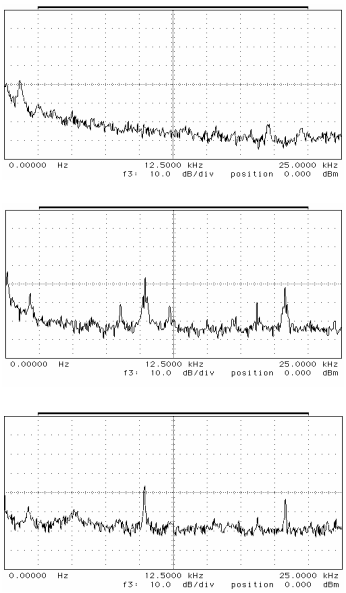

(a)

(b)

(c)

Fig. 13 Frequency spectrum of the switching leg (a) Hysteresis-based torque and flux controllers, (b) Proposed torque and hysteresis-based flux controllers, (c) Proposed torque and flux controllers

V. REFERENCES

[1] I. Takahashi, T. Noguchi, (1986) "A new quick-response and high efficiency control strategy of an induction motor", IEEE Trans. Ind. Appl., Vol. IA-22, No 5, pp. 820-827.

[2] J-K. Kang, D-W Chung and S.K. Sul, (1999) "Direct torque control of induction machine with variable amplitude control of flux and torque hysteresis bands", International Conference on Electric Machines and Drives IEMD'99, pp. 640-642.

[3] Y. Li, J. Shao and B. Si, (1997) "Direct torque control of induction motors for low speed drives considering discrete effect of control and dead-time timing of inveters", IEEE-IAS Annual Meeting, pp. 781-788.

[4] Lixin Tan and M.F. Rahman, (2001) "A new direct torque control strategy for flux and torque ripple reduction for induction motors drive by using space vector modulation", 32nd Annual Power Electronics Specialists Conference PESC. 2001, Vol.3, pp. 1440-1445.

[5] S. Mir, and M. E. Elbuluk, (1995) "Precision torque control in inverter-fed induction machines using fuzzy logic", IEEE-IAS Annual Meeting, pp. 396-401.

[6] N. R. N. Idris, A. H. M. Yatim, (2000) "Reduced torque ripple and constant torque switching frequency strategy for Direct Torque Control of induction machine", 15th IEEE-Applied Power Electronics Conference and Exhibition 2000 (APEC 2000), New Orleans, USA.